

Mask to Adapt: Simple Random Masking Enables Robust Continual Test-Time Learning

Chandler Timm Cagmat Doloriel
Norwegian University of Life Sciences

chandler.timm.cagmat.doloriel@nmbu.no

Abstract

Distribution shifts at test time degrade image classifiers. Recent continual test-time adaptation (CTTA) methods use masking to regulate learning, but often depend on calibrated uncertainty or stable attention scores and introduce added complexity. We ask: do we need custom-made masking designs, or can a simple random masking schedule suffice under strong corruption? We introduce Mask to Adapt (M2A), a simple CTTA approach that generates a short sequence of masked views (spatial or frequency) and adapts with two objectives: a mask consistency loss that aligns predictions across different views and an entropy minimization loss that encourages confident outputs. Motivated by masked image modeling, we study two common masking families—spatial masking and frequency masking—and further compare subtypes within each (spatial: patch vs pixel; frequency: all vs low vs high). On CIFAR10C/CIFAR100C/ImageNetC (severity 5), M2A (Spatial) attains 8.3%/19.8%/39.2% mean error, outperforming or matching strong CTTA baselines, while M2A (Frequency) lags behind. Ablations further show that simple random masking is effective and robust. These results indicate that a simple random masking schedule, coupled with consistency and entropy objectives, is sufficient to drive effective test-time adaptation without relying on uncertainty or attention signals.

1 Introduction

Distribution shifts at test time can severely degrade the performance of image classifiers. A long line of work has explored how to adapt models on-the-fly, often by using unlabeled test data. Early semi-supervised ideas like Pseudo-Labeling Lee (2013) showed that confidence can bootstrap learning without ground-truth labels. Robustness benchmarks Hendrycks & Dietterich (2018) then provided standardized corruptions to stress-test models and quantify their brittleness under realistic noise, blur, weather, and digital artifacts. Building on these foundations, Test-Time Adaptation (TTA) emerged as a practical paradigm: Tent Wang et al. (2021) introduced entropy minimization during testing to push predictions toward confident outputs; CoTTA Wang et al. (2022) studied continual adaptation across evolving domains; VDP Gan et al. (2023) explored visual prompts to steer features; SAR Niu et al. (2023) improved stability under dynamic conditions; PETAL Brahma & Rai (2023) brought a probabilistic view to lifelong TTA; and ViDA Liu et al. (2024b) leveraged adapters to balance domain-specific and domain-shared knowledge.

Recent continual test-time adaptation (CTTA) methods directly use masking as a mechanism to regulate learning under shift. Continual-MAE Liu et al. (2024a) proposes distribution-aware masking for robust representation learning, while Ranked Entropy Minimization (REM) Han et al. (2025) uses attention-based masking of tokens and enforces consistency across masked views. At the same time, these masking-based CTTA methods expose two practical limitations that can hinder reliability under strong corruption: (i) dependence on the quality of model-derived signals—distribution-aware masking requires well-calibrated uncertainty estimates (as in Continual-MAE Liu et al. (2024a)), and attention-based masking relies on stable attention scores (as in REM Han et al. (2025)); (ii) added complexity from computing and maintaining these signals (e.g., extra modules, custom-made scoring pipelines, and tuning schedules). These methods motivate our approach, but leave open a key question: **do we need custom-made masking designs—or can a simple random masking schedule suffice under strong corruption?**

We propose Mask to Adapt (M2A), a simple masking-based CTTA approach designed with these limitations in mind. Given an input, we generate a short sequence of masked views, and adapt with two objectives: a mask consistency loss that aligns predictions across different views and an entropy minimization loss that encourages confident outputs.

Motivated by masked image modeling (MIM), we investigate two common families of masking—spatial masking Bao et al. (2022); He et al. (2021); Xie et al. (2021); Wei et al. (2021) and frequency masking Xie et al. (2023); Wang et al. (2023); Monsefi et al. (2025). We further compare subtypes within each family: for spatial masking, patch-based vs pixel-wise; for frequency masking, masking over all vs low vs high frequencies.

2 Related Work

2.1 Test-Time Adaptation

Early efforts used unlabeled data to improve predictions at test time: Pseudo-Labeling Lee (2013) leveraged model confidence to create labels, standardized robustness benchmarks such as ImageNet-C Hendrycks & Dietterich (2018) quantified failures under common corruptions, and Tent Wang et al. (2021) framed adaptation as entropy minimization to produce confident outputs on corrupted inputs. As focus shifted from single domains to evolving streams, **Continual Test-Time Adaptation** (CTTA) emerged: CoTTA Wang et al. (2022) addressed error accumulation and forgetting; VDP Gan et al. (2023) adapted via visual prompts while keeping the source fixed; SAR Niu et al. (2023) improved stability under mixed shifts and small batches; PETAL Brahma & Rai (2023) reduced drift with a probabilistic teacher-student view; and ViDA Liu et al. (2024b) introduced adapters to balance domain-specific and shared knowledge, aiming to maintain performance as the target distribution changes online.

More recently, CTTA organizes adaptation via masked views. Continual-MAE Liu et al. (2024a) uses distribution-aware masking with consistency to learn robust features under shift, while REM Han et al. (2025) ranks views by difficulty and enforces cross-view agreement to stabilize entropy minimization. These works show that shaping a curriculum over test-time views can improve robustness to corruptions and non-stationary targets; our study follows this line but asks whether a simple random masking schedule can suffice without heavy scoring or complex machinery.

2.2 Masked Image Modelling

Masked image modelling (MIM) has emerged as a strong pre-training paradigm in both spatial and frequency domains. In the spatial domain, BEiT Bao et al. (2022) introduced a token-based objective for masked patches and MAE He et al. (2021) simplified training by masking a high fraction of patches with an asymmetric encoder-decoder, showing that large random masks learn useful features; follow-ups reduced complexity while retaining transfer, with SimMIM Xie et al. (2021) demonstrating that simple random masking and raw-pixel regression with a light head are competitive, and MaskFeat Wei et al. (2021) predicting hand-crafted features to improve efficiency. In the frequency domain, MFM Xie et al. (2023) masked frequency components and predicted the missing spectrum, FreMIM Wang et al. (2023) added multi-stage supervision for dense tasks, and FOLK Monsefi et al. (2025) adaptively selected frequencies and used distillation to reduce the gap to natural inputs; together, these works report competitive performance and robustness without heavy design.

Building on these ideas, recent CTTA methods adopt custom masking for online adaptation. Continual-MAE Liu et al. (2024a) uses distribution-aware masking with consistency to handle changing targets, while REM Han et al. (2025) applies attention-based masking, orders views by difficulty, and enforces cross-view agreement to stabilize entropy minimization. Our study instead asks whether a simple random masking schedule, paired with basic consistency and entropy objectives, can already deliver strong robustness to common corruptions under continual test-time shift.

3 Method

3.1 Problem Setup

Let $f_\theta : [0, 1]^{C \times H \times W} \rightarrow \mathbb{R}^K$ be a classifier with parameters θ . For an input image $x \in [0, 1]^{C \times H \times W}$, the model outputs logits $z = f_\theta(x) \in \mathbb{R}^K$ and class probabilities $p = \text{softmax}(z) \in \Delta^{K-1}$. We receive an *unlabeled* target stream and update θ online at test time, without access to target labels.

Given a positive integer n (number of masking views) and a mask step $\alpha \in (0, 1)$, we define an increasing masking schedule $m_t = t\alpha$ for $t \in \{0, \dots, n-1\}$ with $m_0 = 0$. For each m_t , we construct a masked view $x^{(t)}$ of x , forward it to obtain $z^{(t)} = f_\theta(x^{(t)})$ and $p^{(t)} = \text{softmax}(z^{(t)})$.

3.2 Spatial Masking

For each difficulty level t , we construct a binary spatial mask $M^{(t)} \in \{0, 1\}^{H \times W}$ that determines which spatial locations are removed. The masked view is $x^{(t)} = x \odot (\mathbf{1} - \tilde{M}^{(t)})$, $\tilde{M}^{(t)} := \text{broadcast}_C(M^{(t)}) \in \{0, 1\}^{C \times H \times W}$, where \odot denotes elementwise multiplication, $\mathbf{1}$ is the all-ones tensor, and broadcast_C copies the 2D mask to all C channels. We focus on two binary spatial masking mechanisms.

Patch-based. Let $m_t \in [0, 1]$ be the target masked-area fraction at difficulty level t . We construct a masked index set $\mathcal{A}^{(t)}$ by sampling a collection of axis-aligned square regions $\{\mathcal{R}_\ell\}_{\ell=1}^{P_t}$ whose (possibly overlapping) union approximates the target area:

$$\mathcal{A}^{(t)} := \bigcup_{\ell=1}^{P_t} \mathcal{R}_\ell, \quad \mathcal{A}^{(t)} \subseteq \{0, \dots, H-1\} \times \{0, \dots, W-1\}, \quad |\mathcal{A}^{(t)}| \approx m_t HW. \quad (1)$$

Here, $\ell \in \{1, \dots, P_t\}$ indexes the sampled square regions, and P_t denotes the number of sampled square regions at difficulty level t . Each square is placed at a random grid-aligned location, with side lengths (or counts) chosen to meet the target area budget. The binary mask is $M^{(t)}(i, j) = \mathbf{1}[(i, j) \in \mathcal{A}^{(t)}]$, $(i, j) \in \{0, \dots, H-1\} \times \{0, \dots, W-1\}$. The masked view is $x^{(t)} = x \odot (\mathbf{1} - \tilde{M}^{(t)})$, which removes whole square patches across all channels.

Pixel-wise. To mask individual pixels uniformly at random, we again construct a masked index set $\mathcal{A}^{(t)}$ but now by sampling exactly $k_t = \lfloor m_t HW \rfloor$ pixel locations without replacement. We define $\mathcal{A}^{(t)}$ as a uniformly random subset of spatial positions of size k_t :

$$\mathcal{A}^{(t)} \sim \text{Unif}\left(\left\{\mathcal{S} \subseteq \{0, \dots, H-1\} \times \{0, \dots, W-1\} : |\mathcal{S}| = k_t\right\}\right). \quad (2)$$

The binary mask is therefore $M^{(t)}(i, j) = \mathbf{1}[(i, j) \in \mathcal{A}^{(t)}]$, $(i, j) \in \{0, \dots, H-1\} \times \{0, \dots, W-1\}$. The masked view $x^{(t)} = x \odot (\mathbf{1} - \tilde{M}^{(t)})$ removes the selected pixels independently of neighborhood structure, producing a fine-grained occlusion whose expected masked fraction is m_t .

3.3 Frequency Masking

We apply frequency-domain masking channel-wise using the 2D FFT. For a single channel image $x \in \mathbb{R}^{H \times W}$ with spatial indices (i, j) and frequency indices (u, v) , the 2D FFT and its inverse (computed in practice by the FFT algorithm) are $X[u, v] = \sum_{i=0}^{H-1} \sum_{j=0}^{W-1} x[i, j] \exp(-i 2\pi(\frac{ui}{H} + \frac{vj}{W}))$ and $x[i, j] = \frac{1}{HW} \sum_{u=0}^{H-1} \sum_{v=0}^{W-1} X[u, v] \exp(+i 2\pi(\frac{ui}{H} + \frac{vj}{W}))$. For a color image, these transforms are applied independently to each channel $c \in \{1, \dots, C\}$, producing spectra X_c .

Given a binary spectral mask $M^{(t)} \in \{0, 1\}^{H \times W}$, we zero out selected frequency bins and reconstruct by inverse FFT: $\tilde{X}_c^{(t)}[u, v] = M^{(t)}[u, v] X_c[u, v]$, $x_c^{(t)} = \text{IFFT}(\tilde{X}_c^{(t)})$. We parameterize $M^{(t)}$ by selecting a set of indices $\mathcal{A}_t \subseteq \{0, \dots, H-1\} \times \{0, \dots, W-1\}$ of cardinality $k_t = \lceil m_t HW \rceil$ to be zeroed: $M^{(t)}[u, v] = 1 - \mathbf{1}[(u, v) \in \mathcal{A}_t]$. We consider three selection policies for \mathcal{A}_t :

All Frequency. Uniform random masking over the full spectrum, ablating frequency content across orientations and scales:

$$\Omega_{\text{all}} := \{0, \dots, H-1\} \times \{0, \dots, W-1\}, \quad \mathcal{A}_t \subseteq \Omega_{\text{all}}, \quad |\mathcal{A}_t| = k_t. \quad (3)$$

Low Frequency. Masking restricted to the low-frequency quadrant (no FFT shift; upper-left in array order), attenuating coarse structure and illumination while preserving fine detail:

$$\Omega_{\text{low}} := \{0, \dots, \lfloor H/2 \rfloor - 1\} \times \{0, \dots, \lfloor W/2 \rfloor - 1\}, \quad \mathcal{A}_t \subseteq \Omega_{\text{low}}, \quad |\mathcal{A}_t| = k_t. \quad (4)$$

High Frequency. Masking restricted to the high-frequency quadrant (no FFT shift; lower-right in array order), suppressing textures and edges while retaining coarse global structure:

$$\Omega_{\text{high}} := \{\lfloor H/2 \rfloor, \dots, H-1\} \times \{\lfloor W/2 \rfloor, \dots, W-1\}, \quad \mathcal{A}_t \subseteq \Omega_{\text{high}}, \quad |\mathcal{A}_t| = k_t. \quad (5)$$

3.4 Loss Functions

We write $H(p)$ for the Shannon entropy and $H(p, q)$ for the cross-entropy between distributions $p, q \in \Delta^{K-1}$. The operator $\text{sg}(\cdot)$ denotes stop-gradient.

Mask Consistency. We enforce consistency by aligning masked-view predictions to earlier views (including the unmasked anchor), with the targets detached:

$$\mathcal{L}_{\text{MCL}} = \sum_{t=1}^{n-1} H(p^{(t)}, \text{sg}(p^{(0)})) + \sum_{1 \leq r < t \leq n-1} H(p^{(t)}, \text{sg}(p^{(r)})). \quad (6)$$

Entropy Minimization. We encourage confident predictions on all masking levels by minimizing the average entropy across views:

$$\mathcal{L}_{\text{EML}} = \frac{1}{n} \sum_{t=0}^{n-1} H(p^{(t)}), \quad H(p) = - \sum_{k=1}^K p_k \log p_k. \quad (7)$$

Total Loss. The overall test-time objective adds the two terms: $\mathcal{L}_{\text{TTA}} = \mathcal{L}_{\text{MCL}} + \mathcal{L}_{\text{EML}}$.

4 Experiments

4.1 Dataset

We run experiments on CIFAR10-to-CIFAR10C, CIFAR100-to-CIFAR100C, and ImageNet-to-ImageNetC. The source dataset is CIFAR Krizhevsky et al. (2009) and ImageNet Deng et al. (2009), and the targets are the corrupted versions, CIFAR10C, CIFAR100C, and ImageNetC, built from the common corruption benchmark Hendrycks & Dietterich (2018). Each corrupted set contains 15 corruption types, each with 5 severity levels. Following prior work Wang et al. (2022); Liu et al. (2024b;a); Han et al. (2025), we use the highest severity level (5) for all 15 corruptions and evaluate online classification error after adaptation for each target domain.

Corruption label abbreviations used in figures: GN (Gaussian noise), SN (Shot noise), IN (Impulse noise), DB (Defocus blur), GB (Glass blur), MB (Motion blur), ZB (Zoom blur), S (Snow), Fr (Frost), F (Fog), B (Brightness), C (Contrast), ET (Elastic transform), P (Pixelate), JC (JPEG compression).

4.2 Implementation Details

We evaluate several CTTA baselines with a ViT-B/16 backbone Dosovitskiy et al. (2021) trained on the source data. Baselines include Pseudo-label Lee (2013), Tent Wang et al. (2021), VDP Gan et al. (2023), SAR Niu et al. (2023), CoTTA Wang et al. (2022), PETAL Brahma & Rai (2023), ViDA Liu et al. (2024b), Continual-MAE Liu et al. (2024a), and REM Han et al. (2025). We also show a supervised upper bound trained with target labels (cross-entropy), which is not available in TTA. We run all CIFAR10C, CIFAR100C, and ImageNetC experiments using the open-source REM code Han et al. (2025) and its released source-model weights.

Default hyperparameters. Unless stated otherwise, we use one gradient step per batch; Adam optimizer with learning rate 10^{-3} for CIFAR10C, CIFAR100C, and ImageNetC; weight decay 0.0; mask step $\alpha = 0.1$ between views; number of masking views $n = 3$; and batch size 20. All experiments were run on a single AMD Instinct MI200 GPU.

4.3 Results

4.3.1 Masking Types

We compare classification error rates across masking configurations using the per-dataset panels in Fig. 1: (a) CIFAR10C and (b) CIFAR100C; in each panel, the *left* radar shows spatial masking with the two binary mechanisms from Section 3 (patch-based vs pixel-wise), and the *right* radar shows frequency masking with the three policies (All, Low, High) defined by the spectral index sets in Section 3. Across CIFAR10C and CIFAR100C, two consistent trends emerge: **Spatial**

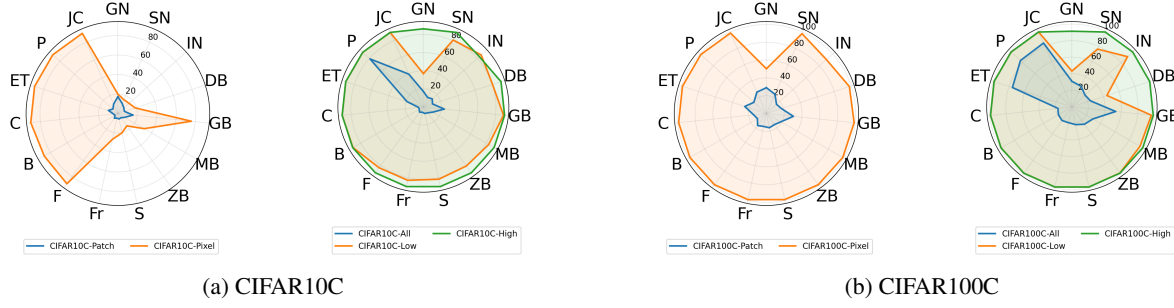


Figure 1: Radar plots of masking types in classification error rate (%). Each subfigure shows spatial masking (Patch/Pixel) and frequency masking (All/Low/High). (a) CIFAR10C. (b) CIFAR100C.

Table 1: Classification error rate (%) on CIFAR10 \rightarrow CIFAR10C under CTTA. Mean is the average across 15 corrupted domains. Gain is the relative improvement over the source model.

Time	$t \rightarrow$															Mean \downarrow	Gain
Method	GN	SN	IN	DB	GB	MB	ZB	S	Fr	F	B	C	ET	P	JC		
Source Dosovitskiy et al. (2021)	60.1	53.2	38.3	19.9	35.5	22.6	18.6	12.1	12.7	22.8	5.3	49.7	23.6	24.7	23.1	28.2	0.0
Pseudo-label Lee (2013)	59.8	52.5	37.2	19.8	35.2	21.8	17.6	11.6	12.3	20.7	5.0	41.7	21.5	25.2	22.1	26.9	+1.3
Tent Wang et al. (2021)	57.7	56.3	29.4	16.2	35.3	16.2	12.4	11.0	11.6	14.9	4.7	22.5	15.9	29.1	19.5	23.5	+4.7
CoTTA Wang et al. (2022)	58.7	51.3	33.0	20.1	34.8	20	15.2	11.1	11.3	18.5	4.0	34.7	18.8	19.0	17.9	24.6	+3.6
VDP Gan et al. (2023)	57.5	49.5	31.7	21.3	35.1	19.6	15.1	10.8	10.3	18.1	4.0	27.5	18.4	22.5	19.9	24.1	+4.1
SAR Niu et al. (2023)	54.1	47.6	38.0	19.9	34.8	22.6	18.6	12.1	12.7	22.8	5.3	39.9	23.6	24.7	23.1	26.6	+1.6
PETAL Brahma & Rai (2023)	59.9	52.3	36.1	20.1	34.7	19.4	14.8	11.5	11.2	17.8	4.4	29.6	17.6	19.2	17.3	24.4	+3.8
ViDA Liu et al. (2024b)	52.9	47.9	19.4	11.4	31.3	13.3	7.6	7.6	9.9	12.5	3.8	26.3	14.4	33.9	18.2	20.7	+7.5
Continual-MAE Liu et al. (2024a)	30.6	18.9	11.5	10.4	22.5	13.9	9.8	6.6	6.5	8.8	4.0	8.5	12.7	9.2	14.4	12.6	+15.6
REM Han et al. (2025)	17.3	12.5	10.3	8.4	17.7	8.4	5.5	6.6	5.6	7.2	3.7	6.4	11.0	7.3	13.0	9.4	+18.8
M2A (Frequency)	17.0 \pm 0.1	11.3 \pm 0.2	13.0 \pm 0.4	10.8 \pm 0.2	23.6 \pm 0.8	11.6 \pm 0.2	8.0 \pm 0.1	7.5 \pm 0.1	6.2 \pm 0.2	7.0 \pm 0.3	5.2 \pm 0.1	5.4 \pm 0.2	18.6 \pm 1.4	78.1 \pm 1.6	49.1 \pm 15.1	18.2	+10.0
M2A (Spatial)	16.9 \pm 0.3	11.2 \pm 0.1	8.3 \pm 0.2	7.2 \pm 0.3	15.6 \pm 0.2	7.7 \pm 0.2	5.2 \pm 0.1	5.8 \pm 0.1	4.7 \pm 0.1	6.1 \pm 0.1	3.6 \pm 0.1	4.9 \pm 0.3	10.2 \pm 0.0	6.9 \pm 0.1	10.6 \pm 0.1	8.3	+19.9
Supervised	14.6	9.0	6.9	6.1	11.2	6.0	3.7	4.4	3.4	4.9	2.1	3.7	7.5	4.3	8.5	6.4	+21.8

Table 2: Classification error rate (%) on CIFAR100 \rightarrow CIFAR100C under CTTA. Mean is the average across 15 corrupted domains. Gain is the relative improvement over the source model.

Time	$t \rightarrow$															Mean \downarrow	Gain
Method	GN	SN	IN	DB	GB	MB	ZB	S	Fr	F	B	C	ET	P	JC		
Source Dosovitskiy et al. (2021)	55.0	51.5	26.9	24.0	60.5	29.0	21.4	21.1	25.0	35.2	11.8	34.8	43.2	56.0	35.9	35.4	0.0
Pseudo-label Lee (2013)	53.8	48.9	25.4	23.0	58.7	27.3	19.6	20.6	23.4	31.3	11.8	28.4	39.6	52.3	33.9	33.2	+2.2
Tent Wang et al. (2021)	53.0	47.0	24.6	22.3	58.5	26.5	19.0	21.0	23.0	30.1	11.8	25.2	39.0	47.1	33.3	32.1	+3.3
CoTTA Wang et al. (2022)	55.0	51.3	25.8	24.1	59.2	28.9	21.4	21.0	24.7	34.9	11.7	31.7	40.4	55.7	35.6	34.8	+0.6
VDP Gan et al. (2023)	54.8	51.2	25.6	24.2	59.1	28.8	21.2	20.5	23.3	33.8	7.5	11.7	32.0	51.7	35.2	32.0	+3.4
SAR Niu et al. (2023)	39.4	31.0	19.8	20.9	43.9	22.6	19.1	20.3	20.2	24.3	11.8	22.3	35.2	32.1	30.1	26.2	+9.2
PETAL Brahma & Rai (2023)	49.2	38.7	24.1	26.3	38.2	25.4	19.4	21.0	19.3	26.6	15.4	31.8	28.3	26.6	29.5	28.0	+7.4
ViDA Liu et al. (2024b)	50.1	40.7	22.0	21.2	45.2	21.6	16.5	17.9	16.6	25.6	11.5	29.0	29.6	34.7	27.1	27.3	+8.1
Continual-MAE Liu et al. (2024a)	48.6	30.7	18.5	21.3	38.4	22.2	17.5	19.3	18.0	24.8	13.1	27.8	31.4	35.5	29.5	26.4	+9.0
REM Han et al. (2025)	29.2	25.5	17.0	19.1	35.2	21.2	18.3	19.5	18.7	22.8	15.5	17.6	31.6	26.2	33.0	23.4	+12.0
M2A (Frequency)	30.5 \pm 0.3	27.3 \pm 0.6	21.7 \pm 0.4	23.6 \pm 0.2	47.7 \pm 4.9	28.2 \pm 1.1	25.1 \pm 0.9	22.1 \pm 0.5	18.9 \pm 0.6	19.8 \pm 0.6	18.6 \pm 0.3	16.8 \pm 0.3	68.3 \pm 19.3	83.7 \pm 6.0	79.3 \pm 7.2	34.4	+1.0
M2A (Spatial)	29.7 \pm 0.8	24.6 \pm 1.0	15.7 \pm 0.4	18.1 \pm 0.2	30.6 \pm 0.5	19.0 \pm 0.2	15.3 \pm 0.1	16.2 \pm 0.2	15.2 \pm 0.3	16.8 \pm 0.1	11.7 \pm 0.2	14.0 \pm 0.3	25.7 \pm 0.6	18.9 \pm 0.1	26.1 \pm 0.3	19.8	+15.6
Supervised	26.2	20.6	13.9	15.9	24.6	15.6	11.8	13.1	12.1	13.6	8.5	9.7	20.2	13.5	21.5	16.1	+19.3

masking (patch-based) yields lower error than pixel-wise masking across most corruptions, suggesting structured occlusions (grid-aligned squares) are a more stable perturbation than randomly scattered pixel drops; **Frequency masking** over *All* frequencies outperforms masking restricted to *Low* or *High* bands, indicating that distributing the mask budget across the spectrum provides a more balanced difficulty signal. Motivated by these results, we adopt *patch-based* masking as default for M2A (Spatial) and *All-frequency* masking as default for M2A (Frequency) in all subsequent experiments.

4.3.2 Comparison with State-of-the-Art

We compare our simple random-masking approach, *Mask to Adapt* (M2A), against prior test-time adaptation baselines and recent masking-based state-of-the-art methods, Continual-MAE Liu et al. (2024a) and REM Han et al. (2025) (Tabs. 1,2,3). M2A comprises two instantiations consistent with Section 3: *M2A (Spatial)* uses binary patch-based masking in the image plane; *M2A (Frequency)* uses all-frequency masking in the spectral domain.

Table 3: Classification error rate (%) for ImageNet-to-ImageNetC under CTTA scenario. Mean (%) denotes the average error rate across 15 target domains. Gain (%) represents the relative performance improvement compared to the source model.

Time	$t \rightarrow$															Mean _t	Gain
Method	GN	SN	IN	DB	GB	MB	ZB	S	Fr	F	B	C	ET	P	JC		
Source Dosovitskiy et al. (2021)	53.0	51.8	52.1	68.5	78.8	58.5	63.3	49.9	54.2	57.7	26.4	91.4	57.5	38.0	36.2	55.8	0.0
Pseudo-label Lee (2013)	45.2	40.4	41.6	51.3	53.9	45.6	47.7	40.4	45.7	93.8	98.5	99.9	99.9	98.9	99.6	61.2	-5.4
Tent Wang et al. (2021)	52.2	48.9	49.2	65.8	73.0	54.5	58.4	44.0	47.7	50.3	23.9	72.8	55.7	34.4	33.9	51.0	+4.8
CoTTA Wang et al. (2022)	52.9	51.6	51.4	68.3	78.1	57.1	62.0	48.2	52.7	55.3	25.9	90.0	56.4	36.4	35.2	54.8	+1.0
VDP Gan et al. (2023)	52.7	51.6	50.1	58.1	70.2	56.1	58.1	42.1	46.1	45.8	23.6	70.4	54.9	34.5	36.1	50.0	+5.8
SAR Niu et al. (2023)	49.3	43.8	44.9	58.2	60.9	46.1	51.8	41.3	44.1	41.8	23.8	57.2	49.9	32.9	32.7	45.2	+10.6
PETAL Brahma & Rai (2023)	52.1	48.2	47.5	66.8	74.0	56.7	59.7	46.8	47.2	52.7	26.4	91.3	50.7	32.3	32.0	52.3	+3.5
ViDA Liu et al. (2024b)	47.7	42.5	42.9	52.2	56.9	45.5	48.9	38.9	42.7	40.7	24.3	52.8	49.1	33.5	33.1	43.4	+12.4
Continual-MAE Liu et al. (2024a)	46.3	41.9	42.5	51.4	54.9	43.3	40.7	34.2	35.8	64.3	23.4	60.3	37.5	29.2	31.4	42.5	+13.3
REM Han et al. (2025)	43.5	38.1	39.2	53.2	49.0	43.5	42.8	37.5	35.2	35.4	23.2	46.8	41.6	28.9	30.2	39.2	+16.6
M2A (Frequency)	45.2 \pm 0.2	42.0 \pm 0.2	43.6 \pm 0.1	62.3 \pm 0.7	53.2 \pm 0.5	51.4 \pm 0.5	78.7 \pm 4.4	51.8 \pm 2.4	61.5 \pm 10.1	40.9 \pm 4.0	26.0 \pm 1.5	62.4 \pm 16.3	76.0 \pm 10.8	75.0 \pm 22.5	59.9 \pm 26.7	55.3	+0.5
M2A (Spatial)	43.4\pm0.1	38.3 \pm 0.1	39.4 \pm 0.1	54.8 \pm 0.7	49.4 \pm 0.7	42.9\pm0.4	43.1 \pm 0.3	36.1 \pm 0.3	35.9 \pm 0.1	35.0\pm0.5	22.5\pm0.1	47.4 \pm 0.4	40.7 \pm 0.6	28.5\pm0.1	29.9\pm0.2	39.2	+16.6
Supervised	42.5	36.9	37.1	46.4	44.0	37.4	38.3	34.2	33.1	32.5	21.5	43.3	34.4	26.1	27.5	35.7	+20.1

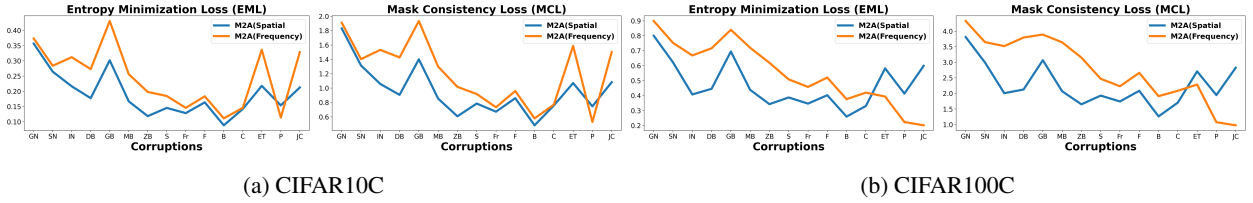


Figure 2: Average loss per corruption for **Entropy Minimization Loss (EML, left panels)** and **Mask Consistency Loss (MCL, right panels)** during adaptation. Each plot shows two lines: M2A (Spatial) and M2A (Frequency). Left: CIFAR10C; Right: CIFAR100C.

On CIFAR10C and CIFAR100C, **M2A (Spatial)** achieves the best mean errors of **8.3%** and **19.8%**, respectively, outperforming REM (9.4%, 23.4%) and Continual-MAE (12.6%, 26.4%). On ImageNetC, **M2A (Spatial)** is competitive at **39.2%**.

By contrast, **M2A (Frequency)** underperforms on all three benchmarks (CIFAR10C: 18.2%, CIFAR100C: 28.0%, ImageNetC: 55.3%), trailing both earlier methods and the recent state-of-the-art. This aligns with our masking-type analysis (Fig. 1), where spatial patch-based masking provides a more effective and stable perturbation curriculum than frequency masking for continual test-time adaptation.

In summary, although Continual-MAE and REM also leverage masking—via distribution-aware and attention-based designs, respectively—our **M2A (Spatial)** shows that a *simple patch masking* strategy can be surprisingly strong, outperforming them on CIFAR10C and CIFAR100C while remaining competitive on ImageNetC.

4.3.3 Loss Profiles

Across both datasets, the loss traces in Fig. 2 show that, in the per-corruption line plots of Mask Consistency Loss (MCL) and Entropy Minimization Loss (EML), **M2A (Spatial)** attains lower loss values than **M2A (Frequency)** for almost all corruptions, with gaps closing only in the last 2–3 corruptions. This pattern indicates that the MCL term pulls masked student views toward the teacher view effectively, while the EML term makes predictions across all masked views more confident; together, these dynamics provide a stable early-phase adaptation signal that aligns with the overall accuracy gains of **M2A (Spatial)** on CIFAR10C and CIFAR100C and its competitive performance on ImageNetC.

4.3.4 Computational Cost

We compare model complexity and mean classification error on CIFAR10C and CIFAR100C in Table 4. **M2A (Ours)** attains the lowest mean error on both datasets while also using the smallest total parameter count, trainable parameter budget, and FLOPs among recent masking-based CTTA methods. This highlights that, despite the simplicity of our random masking schedule and objectives, M2A can outperform methods that rely on custom masking designs for continual test-time adaptation.

Table 4: Model complexity and mean classification error (%) on CIFAR10C and CIFAR100C under CTTA. Computation is based on a ViT-B/16 backbone with input shape (384, 384, 3). Error is averaged over 15 corruptions.

Method	Total Params	Train Params	FLOPs/image	Forward/image	Error (CIFAR10C) ↓	Error (CIFAR100C) ↓
Source Dosovitskiy et al. (2021)	86.6M	0	55G	1	28.2	35.4
Tent Wang et al. (2021)	86.6M	38.4K	55G	1	23.5	32.1
CoTTA Wang et al. (2022)	86.6M	86M	55G	3-35	24.6	34.8
ViDA Liu et al. (2024b)	93.7M	93.7M	60G	12	20.7	27.3
Continual-MAE Liu et al. (2024a)	86.6M	86M	55G	12	12.6	26.4
REM Han et al. (2025)	86.6M	27.6K	55G	3	9.4	23.4
M2A (Ours)	86.6M	27.6K	55G	3	8.3	19.8

Table 5: M2A (Spatial) ablations on CIFAR10C and CIFAR100C (mean classification error, %). Each subtable contains two panels: left = CIFAR10C, right = CIFAR100C.

(a) Loss Function				(b) Learning Rate				(c) Mask Step α			
CIFAR10C		CIFAR100C		CIFAR10C		CIFAR100C		CIFAR10C		CIFAR100C	
Method	Mean↓	Method	Mean↓	Method	Mean↓	Method	Mean↓	Method	Mean↓	Method	Mean↓
Source	28.2	Source	35.4	Source	28.2	Source	35.4	Source	28.2	Source	35.4
M2A (MCL + EML)	8.3	M2A (MCL + EML)	19.80	M2A (1e-3)	8.34	M2A (1e-3)	19.80	M2A ($\alpha=0.1$)	8.35	M2A ($\alpha=0.1$)	19.80
M2A (MCL)	9.3	M2A (MCL)	95.78	M2A (4e-3)	8.48	M2A (4e-3)	23.90	M2A ($\alpha=0.2$)	8.61	M2A ($\alpha=0.2$)	19.68
M2A (EML)	89.7	M2A (EML)	98.33	M2A (4e-4)	9.82	M2A (4e-4)	20.62	M2A ($\alpha=0.3$)	9.02	M2A ($\alpha=0.3$)	20.14

(d) Mask View n				(e) Gradient Steps				(f) Batch Size			
CIFAR10C		CIFAR100C		CIFAR10C		CIFAR100C		CIFAR10C		CIFAR100C	
Method	Mean↓	Method	Mean↓	Method	Mean↓	Method	Mean↓	Method	Mean↓	Method	Mean↓
Source	28.2	Source	35.4	Source	28.2	Source	35.4	Source	28.2	Source	35.4
M2A ($n=2$)	8.84	M2A ($n=2$)	21.11	M2A (steps=1)	8.35	M2A (steps=1)	19.80	M2A (bs=20)	8.35	M2A (bs=20)	19.80
M2A ($n=3$)	8.35	M2A ($n=3$)	19.80	M2A (steps=2)	7.59	M2A (steps=2)	19.92	M2A (bs=10)	7.84	M2A (bs=10)	19.91
M2A ($n=4$)	8.35	M2A ($n=4$)	19.81	M2A (steps=3)	7.13	M2A (steps=3)	97.29	M2A (bs=5)	7.70	M2A (bs=5)	20.52

4.3.5 Ablation Study

Across sample sizes (10%, 20%, 50%, 100%), Figure 3 shows that **M2A (Spatial)** consistently achieves lower mean error than **M2A (Frequency)** on CIFAR10C (Fig. 3a) and CIFAR100C (Fig. 3b). Moreover, **M2A (Spatial)** improves monotonically with sharper gains at larger fractions (e.g., 50% \rightarrow 100%), whereas **M2A (Frequency)** sees only modest reductions. These trends reinforce that simple random *patch-based* masking provides an effective adaptation curriculum that scales with data while all-frequency masking is comparatively unstable.

Combining objectives is essential, and learning dynamics matter. The joint MCL+EML objective delivers the largest and most reliable gains over the Source baseline (28.2%/35.4%): on CIFAR10C it achieves **8.3%** vs **9.3%** (MCL-only) and **89.7%** (EML-only); on CIFAR100C it reaches **19.8%** while MCL-only and EML-only collapse to **95.78%** and **98.33%**. For optimization, an LR of 10^{-3} offers the best trade-off—**8.34%** (CIFAR10C) and **19.80%** (CIFAR100C)—outperforming 4×10^{-4} (9.82%, 20.62%) and 4×10^{-3} (8.48%, 23.9%).

Mask schedule and compute also shape robustness. Smaller inter-view mask steps work best: on CIFAR10C, $\alpha = 0.1$ yields **8.35%** vs 8.61% ($\alpha = 0.2$) and 9.02% ($\alpha = 0.3$); on CIFAR100C, $\alpha = 0.2$ is slightly better (**19.68%**) than $\alpha = 0.1$ (19.80%), while $\alpha = 0.3$ degrades (20.14%). Increasing masked views helps up to saturation: $n = 2$ gives 8.84%/21.11%, while $n = 3$ and $n = 4$ improve to 8.35%/19.80% and 8.35%/19.81%; we thus default to $n = 3$. Taking more optimizer steps per batch yields mixed effects: on CIFAR10C, $1 \rightarrow 2 \rightarrow 3$ steps improves 8.35% \rightarrow 7.59% \rightarrow 7.13%, but on CIFAR100C it destabilizes (19.80% \rightarrow 19.92% \rightarrow 97.29%), so we use a single step by default. Finally, smaller batches slightly help on CIFAR10C but hurt on CIFAR100C: bs=20/10/5 yields 8.35%/7.84%/7.70% vs 19.80%/19.91%/20.52%; we choose bs=20 as a balanced default that avoids degradation on CIFAR100C while remaining competitive on CIFAR10C.

5 Discussion

5.1 Why random masking works?

Global integration and regularization. Random *patch-based* masking compels the model to use broader spatial support and, together with MCL+EML, acts as a regularizer that discourages shortcut cues tied to localized corruptions. By

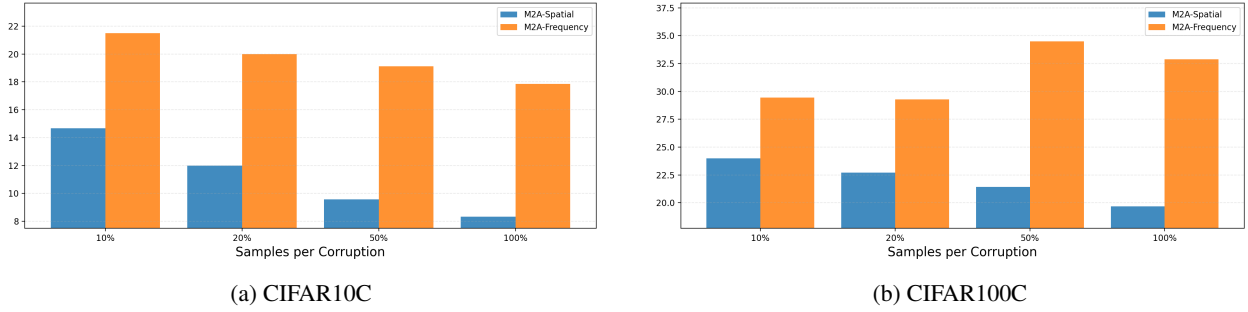


Figure 3: Effect of per-corruption sample size on mean classification error rate for CIFAR10C (a) and CIFAR100C (b). Each plot reports error at 10%, 20%, 50%, and 100% of the available samples per corruption; 100% equals 10k samples in both datasets.

masking different regions across views, the model cannot latch onto brittle, corruption-specific artifacts and is instead pushed to explain inputs via global structure and multi-region evidence. This aligns with Fig. 1 (spatial patch masking outperforming pixel-wise across most corruptions) and with our overall results where **M2A (Spatial)** is stronger and more stable than frequency variants.

Chance removal of worst regions. Under common corruptions, heavily degraded pixels or localized artifacts (e.g., snow, frost, pixelation) can dominate uncertainty. Random occlusions probabilistically drop such regions while preserving sufficient context, yielding cleaner evidence from the remainder of the image. Consistent improvements across many per-corruption columns in Tabs. 1,2,3 reflect this effect, with **M2A (Spatial)** frequently matching or surpassing the best baseline.

Diversity across adaptation steps. A short sequence of independently masked views ($n = 3$) exposes the model to diverse partial observations, and MCL ties their predictions together. Tab. 5 shows that increasing views helps then saturates (CIFAR10C: 8.84% \rightarrow 8.35%; CIFAR100C: 21.11% \rightarrow 19.80%), while Fig. 3 indicates consistent gains as more target samples are seen. This diversity-plus-consistency mechanism enables effective adaptation without bespoke scoring or heavy machinery.

5.2 Why frequency masking underperforms?

Inductive bias. Our baseline is a ViT, whose tokenization and attention operate over image patches. Patch masking respects this spatial token structure and encourages robust aggregation from visible tokens, whereas frequency masking perturbs the signal globally in a basis misaligned with the model’s native representation.

Global information removal and artifacts. Frequency masking can suppress low- or high-frequency bands that carry global structure (object contours, textures), and zeroing bands can introduce ringing or unnatural artifacts after inverse FFT. In Fig. 2, **M2A (Frequency)** shows more volatility, especially near the tail corruptions, while **M2A (Spatial)** stays steadier across the first 11/15 corruptions. The average losses reflect this on CIFAR10C (MCL: **0.86** vs 1.03; EML: **0.14** vs 0.17) and are comparable on CIFAR100C (MCL: 1.94 vs 1.96; EML: 0.38 vs 0.34), indicating that stability—rather than raw loss magnitude—better predicts final accuracy under CTTA.

Selective corruption removal vs semantic erasure. Patch masking randomly occludes localized regions; by chance it often removes heavily corrupted areas (e.g., S/Fr/P/JC) while preserving enough uncorrupted context for recognition. Frequency masking, in contrast, removes dispersed information across the whole image, which can erase semantics even when only a fraction is masked. This aligns with per-corruption improvements in Tabs. 1,2,3 and with the early-phase stability seen in Fig. 2, both favoring spatial patch masking for continual adaptation.

6 Conclusion

We studied continual test-time adaptation (CTTA) under strong corruptions and asked whether custom-made masking is necessary or a simple random masking schedule suffices. Motivated by masked image modeling, we investigated spatial

and frequency masking (patch vs pixel; all vs low vs high) and proposed Mask to Adapt (M2A): a masking schedule that generates a short sequence of progressively masked views and adapts with two objectives—mask consistency across views (MCL) and entropy minimization (EML). M2A avoids uncertainty/attention scoring and plugs into standard ViT-B/16 backbones. Across CIFAR10C/CIFAR100C/ImageNetC (severity 5), M2A (Spatial) achieves 8.3%/19.8%/39.2% mean error, outperforming REM and Continual-MAE on the CIFAR benchmarks and remaining competitive on ImageNetC, while M2A (Frequency) lags (18.2%/28.0%/55.3%). Ablations show MCL+EML is essential and that robust defaults (LR $1e^{-3}$, $\alpha \approx 0.1$, $n = 3$, one step, moderate batch) are effective. Our analysis explains the gains: patch masking promotes global feature integration, regularizes against overfitting, often drops heavily corrupted regions while preserving context, and—through multiple views tied by MCL—yields stable early loss profiles (first 11/15 corruptions). In contrast, frequency masking can remove globally critical information and introduce artifacts misaligned with the model’s spatial inductive bias. Taken together, a simple random patch-masking curriculum with MCL+EML is sufficient for strong, stable CTTA without custom-made scoring.

References

- Hangbo Bao, Li Dong, and Furu Wei. Beit: Bert pre-training of image transformers. *ICLR*, 2022.
- Dhanajit Brahma and Piyush Rai. A probabilistic framework for lifelong test-time adaptation. In *Proceedings of the IEEE/CVF Conference on Computer Vision and Pattern Recognition*, 2023.
- Jia Deng, Wei Dong, Richard Socher, Li-Jia Li, Kai Li, and Li Fei-Fei. Imagenet: A large-scale hierarchical image database. In *Proceedings of the IEEE/CVF Conference on Computer Vision and Pattern Recognition*, pp. 248–255. Ieee, 2009.
- Alexey Dosovitskiy, Lucas Beyer, Alexander Kolesnikov, Dirk Weissenborn, Xiaohua Zhai, Thomas Unterthiner, Mostafa Dehghani, Matthias Minderer, Georg Heigold, Sylvain Gelly, Jakob Uszkoreit, and Neil Houlsby. An image is worth 16x16 words: Transformers for image recognition at scale. In *International Conference on Learning Representations*, 2021.
- Yulu Gan, Yan Bai, Yihang Lou, Xianzheng Ma, Renrui Zhang, Nian Shi, and Lin Luo. Decorate the newcomers: Visual domain prompt for continual test time adaptation. In *Proceedings of the AAAI Conference on Artificial Intelligence*, volume 37, pp. 7595–7603, 2023.
- Jisu Han, Jaemin Na, and Wonjun Hwang. Ranked entropy minimization for continual test-time adaptation. *International Conference on Machine Learning (ICML)*, 2025.
- Kaiming He, Xinlei Chen, Saining Xie, Yanghao Li, Piotr Doll’ar, and Ross B. Girshick. Masked autoencoders are scalable vision learners. *2022 IEEE/CVF Conference on Computer Vision and Pattern Recognition (CVPR)*, 2021.
- Dan Hendrycks and Thomas Dietterich. Benchmarking neural network robustness to common corruptions and perturbations. In *International Conference on Learning Representations*, 2018.
- Alex Krizhevsky, Geoffrey Hinton, et al. Learning multiple layers of features from tiny images. 2009.
- Dong-Hyun Lee. Pseudo-label : The simple and efficient semi-supervised learning method for deep neural networks. In *International conference on machine learning Workshop*, 2013.
- Jiaming Liu, Ran Xu, Senqiao Yang, Renrui Zhang, Qizhe Zhang, Zehui Chen, Yandong Guo, and Shanghang Zhang. Continual-mae: Adaptive distribution masked autoencoders for continual test-time adaptation. *Proceedings of the IEEE/CVF Conference on Computer Vision and Pattern Recognition*, 2024a.
- Jiaming Liu, Senqiao Yang, Peidong Jia, Ming Lu, Yandong Guo, Wei Xue, and Shanghang Zhang. Vida: Homeostatic visual domain adapter for continual test time adaptation. In *International Conference on Learning Representations*, 2024b.
- Amin Karimi Monsefi, Mengxi Zhou, Nastaran Karimi Monsefi, Ser-Nam Lim, Wei-Lun Chao, and Rajiv Ramnath. Frequency-guided masking for enhanced vision self-supervised learning. *ICML*, 2025.

-
- Shuaicheng Niu, Jiaxiang Wu, Yifan Zhang, Zhiquan Wen, Yaofo Chen, Peilin Zhao, and Mingkui Tan. Towards stable test-time adaptation in dynamic wild world. In *International Conference on Learning Representations*, 2023.
- Dequan Wang, Evan Shelhamer, Shaoteng Liu, Bruno A. Olshausen, and Trevor Darrell. Tent: Fully test-time adaptation by entropy minimization. In *International Conference on Learning Representations*, 2021.
- Qin Wang, Olga Fink, Luc Van Gool, and Dengxin Dai. Continual test-time domain adaptation. In *Proceedings of Conference on Computer Vision and Pattern Recognition*, 2022.
- Wenxuan Wang, Jing Wang, Chen Chen, Jianbo Jiao, Lichao Sun, Yuanxiu Cai, Shanshan Song, and Jiangyun Li. Fremim: Fourier transform meets masked image modeling for medical image segmentation. *2024 IEEE/CVF Winter Conference on Applications of Computer Vision (WACV)*, 2023.
- Chen Wei, Haoqi Fan, Saining Xie, Chaoxia Wu, Alan Loddon Yuille, and Christoph Feichtenhofer. Masked feature prediction for self-supervised visual pre-training. *2022 IEEE/CVF Conference on Computer Vision and Pattern Recognition (CVPR)*, 2021.
- Jiahao Xie, Wei Li, Xiaohang Zhan, Ziwei Liu, Yew Soon Ong, and Chen Change Loy. Masked frequency modeling for self-supervised visual pre-training. *ICLR*, 2023.
- Zhenda Xie, Zheng Zhang, Yue Cao, Yutong Lin, Jianmin Bao, Zhuliang Yao, Qi Dai, and Han Hu. Simmim: a simple framework for masked image modeling. *2022 IEEE/CVF Conference on Computer Vision and Pattern Recognition (CVPR)*, 2021.